Environmental Science: Atmospheres

ROYAL SOCIETY OF CHEMISTRY

PAPER

View Article Online
View Journal

Cite this: DOI: 10.1039/d5ea00126a

Impact of mixing states on aerosol radiative effects and feedback during winter haze episodes over the North China Plain

Jing Wang, [ab] Zhiwei Han, *[ab] Yunfei Wu, [c] Jiawei Li [a] and Yuanyuan Zheng [d]

An online-coupled regional climate-chemistry-aerosol model (RIEMS-Chem) was developed and applied to investigate the impact of the aerosol mixing state on aerosol-radiation-meteorology feedback during the winter haze episode of 8–13 February 2020 over the North China Plain (NCP). Model validation demonstrates the overall good ability of the model in reproducing the meteorological variables, $PM_{2.5}$ and its components, and aerosol optical properties. Aerosol optical depth (AOD) and single scattering albedo (SSA) simulated with the Maxwell-Garnett mixing assumption are closest to the AERONET observations, whereas external mixing tends to predict lower AOD and higher SSA, in contrast to core–shell mixing and homogeneous mixing, which predict lower SSA. The direct radiative effects (DREs) under various aerosol mixing states differ largely, with the percentage differences of 24% and 40% and a factor of three at the top of the atmosphere (TOA), at the surface and in the atmosphere, respectively, averaged over the haze episode. The sensitivity of the aerosol optical properties and DRE to the black carbon size distribution, coating fraction, and hygroscopic growth under Maxwell-Garnett mixing is also investigated, showing the remarkable effect of hygroscopic growth. During the most severe haze day in Beijing, the changes in air temperature and relative humidity at 2 m (T2, RH2) and wind speed at 10 m (WS10) induced by aerosol radiative feedback vary by −1.2–1.4 °C, 5.5–6.2%, and −0.28–0.37 m s^{-1}, respectively, and the feedback-induced increase in $PM_{2.5}$ concentration varies considerably from 40.3 μg m^{-3} to 57.6 μg m^{-3} across different mixing states. The radiative feedback leads to an increase in $PM_{2.5}$ concentration by 25%, 30%, 30% and 36% under external mixing, Maxwell-Garnett mixing, core–shell mixing and homogeneous mixing states, respectively. It is noteworthy that the aerosol mixing state not only affects the magnitude but also the direction of near-surface air temperature change, depending on the relative magnitude of aerosol-induced atmospheric heating and DRE-induced cooling. The strongest atmospheric heating rate (AHR) under homogeneous mixing leads to an increase in T2 and planetary boundary layer height (PBLH) in portions of southern NCP, which tends to reduce the $PM_{2.5}$ concentration. This study demonstrates the important role of radiative feedback in exacerbating air pollution and the significant impacts of aerosol mixing state on DRE, AHR and radiative feedback during the haze episode.

Received 29th September 2025
Accepted 20th December 2025

DOI: 10.1039/d5ea00126a

rsc.li/esatmospheres

Environmental significance

Aerosol radiative feedback exerts significant effects on meteorology and the near-surface PM2.5 concentration during haze events. Aerosol mixing state is supposed to be an essential factor affecting aerosol radiative effects and feedback but poorly understood and estimated at present. Our results reveal large differences in the magnitude of aerosol direct radiative effects across different mixing states, which lead to diverse feedback effects on meteorology and PM2.5 concentrations. These results will be useful for understanding and predicting air pollution and climate change at both regional and global scales.

1. Introduction

Aerosols can affect radiation transfer and clouds through direct, indirect and semi-direct effects.[1–3] The changes in radiation and cloud properties may in turn provide feedback to meteorology and physical processes (advection/diffusion and depositions) and further alter chemical reactions of gas and aerosols, which

[a]State Key Laboratory of Earth System Numerical Modeling and Application, Institute of Atmospheric Physics, Chinese Academy of Sciences, Beijing 100029, China. E-mail: hzw@mail.iap.ac.cn

[b]College of Earth and Planetary Sciences, University of Chinese Academy of Sciences, Beijing 100049, China

[c]State Key Laboratory of Atmospheric Environment and Extreme Meteorology, Institute of Atmospheric Physics, Chinese Academy of Sciences, Beijing 100029, China

[d]Department of Atmospheric Sciences, Yunnan University, Kunming 650091, China

are highly dependent on temperature, relative humidity, and cloud properties. The above-mentioned aerosol-radiation-cloud-meteorology interaction is very complex and remains one of the least understood mechanisms in air quality and climate research.[4–6]

To explore the underlying mechanism of the abrupt increase in $PM_{2.5}$ concentrations during haze episodes, a number of studies have investigated the role of aerosol radiative feedback in haze formation,[7–20] all of which indicated a positive radiative feedback to increasing $PM_{2.5}$ concentration. However, there were large differences in the magnitude of the feedback effect among model results (with a few percent increase to approximately 40% increase in near-surface $PM_{2.5}$ concentration), which could be related to potential differences in the predictions of meteorological fields, aerosol chemical component levels, and treatments of aerosol mixing states and hygroscopic growth, among which the mixing states of aerosols are considered to be one of the most important factors greatly affecting aerosol optical and radiative properties.[21–23] A number of observational studies were conducted for the NCP, which revealed the sources, properties, evolution processes of black carbon (BC) and the mixing state of BC with other anthropogenic aerosols.[24–28] Several aerosol mixing states were assumed in previous studies to estimate the aerosol feedback on particulate pollution. Wang *et al.*[8] performed simulations using the NAQPMS model and showed that the feedback may enhance the $PM_{2.5}$ levels by 10–30% during the severe haze events in January 2013 in the North China Plain (NCP), with the assumption of external mixing. Wu *et al.*[17] indicated that aerosol radiative effects contributed 12–20% of the near-surface $PM_{2.5}$ concentration during a heavy haze episode in NCP in winter 2015 by using a homogeneous internal mixing assumption in WRF-Chem. Qiu *et al.*[12] estimated the percentage change in $PM_{2.5}$ concentration due to feedback ranging from 8% to approximately 50%, increasing with $PM_{2.5}$ levels during the haze events on 21–27 February 2014, with a core–shell internal mixing assumption in WRF-Chem. Despite the differences in the study periods, meteorology and emissions, the various treatments of the aerosol mixing state in the above-mentioned studies are considered to be one of the key factors determining the large difference in the feedback-induced $PM_{2.5}$ changes; however, thus far, there are very limited studies on the impact of different aerosol mixing states on the radiative feedback effects on $PM_{2.5}$ and meteorology.

In addition, the majority of previous studies only performed model validation for AOD, which just represents a column-integrated aerosol extinction. The lack of model validation for single scattering albedo (SSA), which is a key parameter determining the relative magnitude of aerosol absorption and scattering ability, reduces the reliability of the predicted aerosol radiative effects, and thus feedback.

In the past two decades, haze pollution has been one of the most important environmental issues in China with the continuous growth of the economy and urbanization, which was the most serious in January 2013. Thus, to tackle air pollution, the Chinese government launched a series of air pollution control strategies, which evidently reduced the concentration of fine particulates.[29] However, despite the successful improvement in air quality in China, sporadic haze events still occurred in NCP in winter, even during the COVID-19 epidemic in February 2020, when a haze event occurred in Beijing with the maximum hourly $PM_{2.5}$ concentration exceeding 260 $\mu g\ m^{-3}$. The occurrence of this haze episode was mainly attributed to poor meteorological conditions, while the reduction in anthropogenic emissions due to COVID-19 lockdown led to a slight decrease in $PM_{2.5}$ concentration.[30]

In this study, the RIEMS-Chem model was applied to explore the aerosol-radiation-meteorology interaction and feedback during the haze episode of 8–13 February 2020, to estimate the aerosol direct radiative effects (DRE), and to our knowledge, for the first time to quantify the aerosol radiative feedback on meteorology and near-surface $PM_{2.5}$ concentration under different aerosol mixing states. The results from this study will provide new insights into the aerosol-radiation-meteorology feedback mechanism related to aerosol mixing states, which is currently one of the most important sources of uncertainties in air quality and climate predictions.

2. Model and data

2.1 Model description

This study utilizes an online-coupled regional climate-chemistry-aerosol model, RIEMS-Chem, developed based on the Regional Integrated Earth Modeling System (RIEMS), which is introduced in detail by Fu *et al.*[31] and Wang *et al.*[32] A series of atmospheric chemistry and aerosol processes have been incorporated into RIEMS to establish RIEMS-Chem.[18,33–35] The schemes for the advection and diffusion of chemical species are identical to that for water vapor. An updated Carbon Bond mechanism (CB-IV)[36] is used to represent gas-phase chemical processes, with the photolysis rate calculated using the tropospheric Ultraviolet-Visible (TUV) radiation model.[37] Thermodynamic equilibrium between gases and particles is treated by ISORROPIA II.[38] A two-product model[39] is applied to calculate secondary organic aerosol (SOA) concentration with updated aromatic compound yields. Uptake and chemical reactions of anthropogenic gas precursors, *e.g.*, sulfur dioxide, and nitrogen dioxide on the surfaces of mineral dust, sea salt and hydrated anthropogenic aerosols are represented by the approaches reported by Li and Han[40] and Li *et al.*,[41,42] respectively. Dry deposition and below-cloud scavenging of aerosols is parameterized using the same schemes as Han *et al.*[43]

RIEMS-Chem accounts for major anthropogenic and natural aerosols, *i.e.*, sulfate, nitrate, ammonium, black carbon (BC), primary organic aerosol (POA), secondary organic aerosol (SOA), mineral dust, and sea salt. The size distribution of the different types of aerosols is prescribed mainly based on the OPAC database.[44] Field measurements in Beijing are also used to characterize the size distribution of BC, which show that the mass peak diameter is approximately 210 nm with a lognormal distribution.[26] The size distributions of mineral dust and sea salt are classified into five bins, *i.e.*, 0.1–1.0, 1.0–2.0, 2.0–4.0, 4.0–8.0, and 8.0–20.0 μm. Dust deflation and sea salt generation are parameterized following the approaches reported by Han

et al.[43] and Gong *et al.*[45] Aerosol hygroscopic growth is treated by kappa (κ) parameterization,[46] with the wet radius of aerosols calculated using the Kohler theory. The κ values for inorganic salts, BC, POA, SOA, dust, and sea salts are set to 0.65, 0, 0.1, 0.2, 0.01, and 0.98, respectively, according to previous studies. In this study, mineral dust and sea salt are assumed to be externally mixed with anthropogenic aerosols, while anthropogenic aerosols are assumed to be mixed with each other in four ways, external mixing, Maxwell-Garnett internal mixing, core–shell internal mixing, and homogeneous internal mixing. External mixing denotes that aerosols keep their own properties while mixing with each other, and the optical properties of total aerosols are the sum of their of individual aerosols. Maxwell-Garnett mixing is based on an equivalent medium theory that assumes a coated sphere on a randomly distributed core, where the refractive index of the mixed aerosols is calculated using the Maxwell-Garnett mixing rule.[47,48] Core–shell mixing represents a coated sphere on a concentric core. The optical properties of core–shell mixing aerosols are calculated using an improved Mie program[49] with complex refractive indices and volume ratios of core and shell. Homogeneous mixing means aerosols mix with each other homogeneously, with the refractive index of the mixture calculated using a volume-weighted average approach. In the Maxwell-Garnett and core–shell mixing states, BC is treated as the core, while inorganic aerosols and SOA are taken as the shell.

RIEMS-Chem has been applied to explore a number of environmental issues regarding air pollution, aerosol processes, and aerosol-radiation-cloud-weather/climate interactions over East Asia.[18,19,33–35,50–59]

2.2 Model configuration and numerical experiments

RIEMS-Chem has a horizontal resolution of 60 km and 16 layers in the vertical on a lambert projection. The center of the study domain is located at 110°E and 35°N. The study period is from 27 January to 18 February 2020, covering the haze episode of 8–13 February, during which the observed maximum hourly $PM_{2.5}$ concentration exceeded 260 μg m^{-3}. The first five days are taken as spin-up time. The study domain is shown in Fig. 1, along with the topography and locations of the observational sites.

To quantify the impacts of different aerosol mixing states on aerosol radiative effects and feedback, a series of numerical experiments is designed. The first experiment assumes external mixing (denoted as EXT) of anthropogenic aerosols; the second adopts Maxwell-Garnett internal mixing (denoted as M-G); the third considers core–shell internal mixing (denoted as C–S); and the fourth represents homogeneous internal mixing (denoted as HOM). In each case, the direct radiative effect (DRE) is estimated based on the difference between two radiation calls with and without anthropogenic aerosols (*i.e.* calling twice in the radiation module in one simulation). The feedback effect induced by DRE on meteorological variables and $PM_{2.5}$ concentration is estimated by comparing two simulations with and without aerosol radiative effects (CASE0). In the above-mentioned sensitivity simulations, the initial and boundary meteorological fields, emissions and boundary conditions are

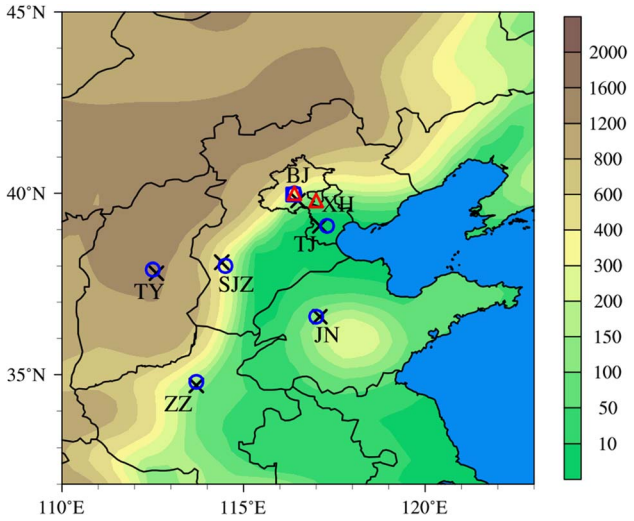

Fig. 1 The study domain with topography (m). Markers are observation sites (black crosses denote the observational sites for meteorological variables; blue circles denote the observational sites for $PM_{2.5}$ concentration; blue square denotes the tower monitoring site of IAP for $PM_{2.5}$ chemical components; and red triangles denote the AERONET sites).

the same. The 1.0° × 1.0°, 6-hourly initial and boundary meteorological conditions are derived from the final reanalysis data (FNL) from the National Centers for Environmental Prediction (NOAA/NCEP, https://rda.ucar.edu/datasets/d083002/). MOZART-4 (Model for Ozone and Related Chemical Tracers, http://www.acd.ucar.edu/wrfchem/mozart.html) provides 6-hourly boundary conditions of chemical species. Indirect radiation effects are not considered in this study due to the limited precipitation and cloud cover during the haze episode, as shown in Fig. S1.

2.3 Emissions and observations

The monthly mean anthropogenic emissions in China are derived from MEIC (http://meicmodel.org/). Biomass burning and biogenic VOC emissions are derived from GFEDv4 (https://www.globalfiredata.org/) and GEIA (http://www.geiacenter.org/), respectively.

Hourly meteorological observations, including 2 m air temperature (T2), 2 m relative humidity (RH2), and 10 m wind speed (WS10), are derived from the National Centers for Environmental Information (NOAA/NCEI, https://www.ncei.noaa.gov/). Hourly $PM_{2.5}$ observations are derived from the China National Environmental Monitoring Centre (http://www.cnemc.cn/). $PM_{2.5}$ component measurements were conducted at the tower branch of the Institute of Atmospheric Physics, Chinese Academy of Sciences (39°58′N, 116°22′E) in Beijing. Ground measurements of aerosol optical depth (AOD) and single scattering albedo (SSA) at the Beijing-RADI and Xianghe sites are derived from AERONET (https://aeronet.gsfc.nasa.gov/). The Beijing-RADI site (40°00′N, 116°24′E) is located in downtown Beijing, while the Xianghe site (39°48′N, 117°00′E) is in the suburb area of Hebei province,

about 60 km southeast of Beijing downtown. Daily satellite-derived AOD and precipitation data are obtained from MODIS (https://ladsweb.modaps.eosdis.nasa.gov/) and GPM (https://gpm.nasa.gov/), respectively.

3. Results

3.1 Model validation with observations

3.1.1 Meteorological variables. Table S1 shows the model performance statistics for meteorological variables in the six megacities in NCP during the study period. The overall model performance is generally good, with the correlation coefficients (R) of 0.89, 0.63, and 0.69 for T2, WS10, and RH2, and the normalized mean biases (NMB) of 0.3%, 7.1%, and 19.8%, respectively. WS10 is somewhat overestimated in Jinan and Taiyuan, while RH2 is overestimated by approximately 30% in Shijiazhuang and Taiyuan. The model reproduces the meteorological variables quite well in Beijing and Tianjin, with NMBs of 0.5–0.6%, −4.9–6.8% and 8.7–11.4% for T2, WS10 and RH2, respectively.

3.1.2 $PM_{2.5}$ concentration and aerosol components. Table 1 presents the model performance statistics for near-surface hourly $PM_{2.5}$ concentrations in the six cities in NCP. The model generally reproduces the $PM_{2.5}$ distribution and variability, with the overall R and NMB being 0.69% and 4%, respectively, for all cities. The model performs better in Beijing, Zhengzhou and Shijiazhuang, with R of 0.55 to 0.88, and NMB of −14% to 12%, whereas the model bias in Taiyuan is relatively large, which could be due to the potential uncertainties in emission inventories and meteorological predictions.

Fig. 2 presents the observed and model simulated hourly concentrations of $PM_{2.5}$ and its chemical components in Beijing during the study period. The model reproduces quite well the temporal variations and magnitudes of $PM_{2.5}$ components from 1 to 18 February, 2020, including the increase in $PM_{2.5}$ and its components during the haze episode from 8 to 13 February. The OC concentration is underpredicted, especially during the haze episode, which could be due to the exclusion of some precursors, *e.g.*, semi-volatile and intermediate-volatile organic compounds and limitation in understanding multiphase SOA formation processes. Table 2 presents the model performance statistics for the $PM_{2.5}$ components in Beijing, which exhibits the generally good ability of the model, with R of 0.80–0.91 and NMB < 24%.

3.1.3 Aerosol optical depth (AOD) and single scattering albedo (SSA). Fig. S2 shows the model-simulated and MODIS retrieved average AOD at 550 nm at 10:30 LST during the haze episode of 8–13 February 2020. The model generally reproduces the distribution pattern of AOD over NCP, with higher values in the areas around Beijing and Tianjin, and the southeastern portions of the domain. The model tends to predict higher AOD than observations in the southern parts of NCP, which could be due to the overpredictions of the relative humidity (Table S1) and $PM_{2.5}$ concentrations (Table 1) in those regions.

Fig. 3 presents the measured and simulated daily mean AOD and SSA at 550 nm at the Beijing-RADI and Xianghe sites during the study period in the four cases. The model reasonably reproduces the day-to-day variation of AOD and SSA, with an increase in the $PM_{2.5}$ concentration during the growth stage of the haze episode of 8–13 February at both sites (there is no observational data at Xianghe on 13 and 14 February), despite some underpredictions at Beijing-RADI. It is noteworthy that the simulated AOD in the four sensitivity cases is close to each other, except for an apparent underprediction in the EXT case, whereas the simulated SSA differs largely among them. The SSA in the EXT case is the highest among the four cases, which means the least absorption, followed by SSA in the M-G and C–S cases, and SSA in the HOM case is the lowest, which means the strongest absorption. It is clearly seen that during the haze episode of 9–12 February, the simulated SSA in M-G agrees best with the observations among the mixing cases, whereas EXT and C–S/HOM tend to overpredict and underpredict SSA, respectively. Previous observational analyses[24,25] reported that anthropogenic aerosols during haze periods in Beijing favored core–shell mixing over homogeneous mixing. The underprediction of SSA in the C–S case compared to the AERONET measurements in this study is consistent with some previous studies, *e.g.*, Fierce *et al.*[60] indicated that a concentric core–shell approximation generally overestimated the field observation of BC absorption. This could explain why the M-G-simulated SSA is the closest to observations because the absorption under M-G mixing is smaller than that with concentric core–shell mixing (in the visible band) due to the weaker lensing effect on a randomly distributed core (lensing effect refers to the coating

Table 1 Model performance statistics for hourly $PM_{2.5}$ concentrations (in the M-G case) in the six major cities over NCP during the study period from 1 to 18 February 2020 (unit: μg m^{-3})

			$PM_{2.5}$				
Cities	Long name	Location	Obs	Sim	R	MB	NMB
BJ	Beijing	116.4°E, 40.0°N	67.5	75.2	0.88	7.7	11.5%
TJ	Tianjin	117.3°E, 39.1°N	62.5	85.0	0.86	22.5	36.0%
SJZ	Shijiazhuang	114.5°E, 38.0°N	84.6	72.7	0.65	−12.0	−14.1%
ZZ	Zhengzhou	113.7°E, 34.8°N	61.5	60.3	0.55	−1.2	−1.9%
TY	Taiyuan	112.5°E, 37.9°N	66.2	42.2	0.48	−24.0	−36.3%
JN	Jinan	117.0°E, 36.6°N	57.0	73.5	0.70	16.5	28.9%
ALL			66.6	68.1	0.69	1.6	4.0%

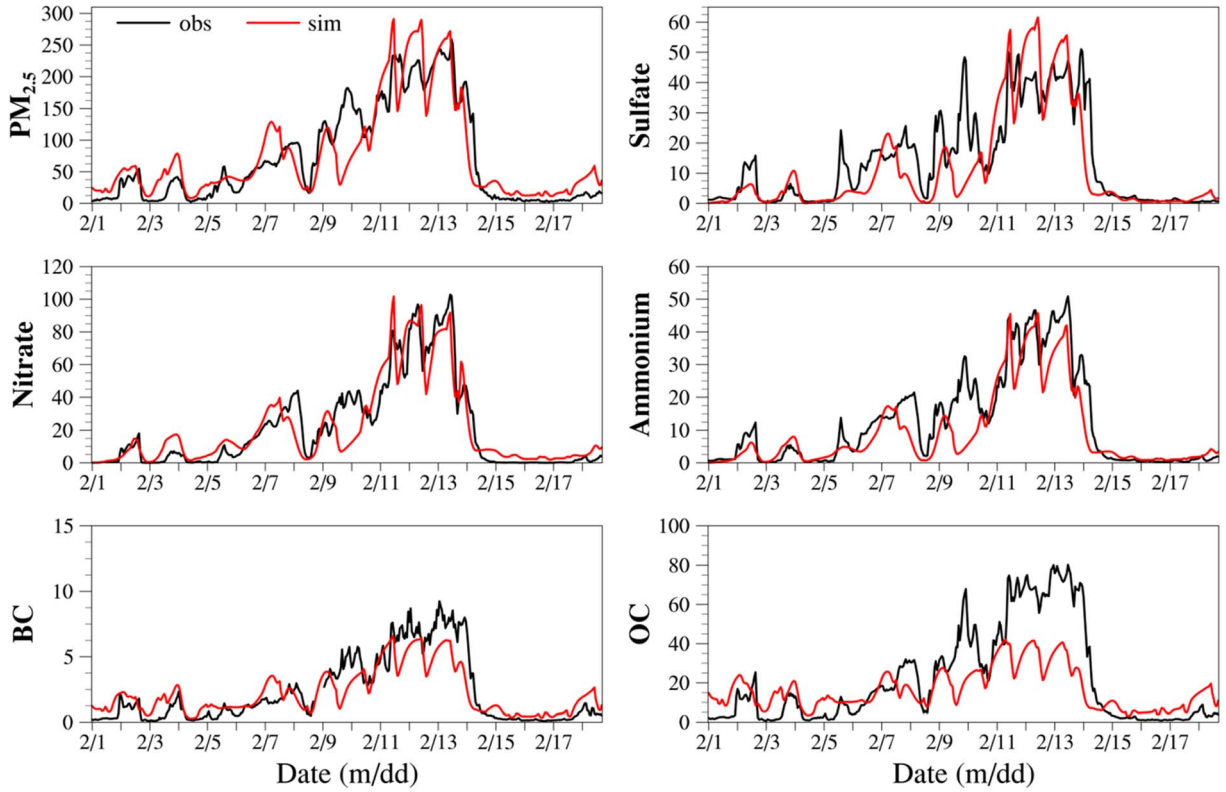

Fig. 2 The observed and model-simulated (from the M-G case) hourly concentrations of $PM_{2.5}$ and its chemical components in Beijing from 1 to 18 February, 2020 (unit: μg m^{-3}).

Table 2 Model performance statistics for hourly $PM_{2.5}$ component concentrations (in the M-G case) in Beijing during the study period from 1 to 18 February 2020 (unit: μg m^{-3})

Component	Obs	Sim	*R*	MB	NMB
SO_4^{2-}	13.6	11.6	0.81	−2.03	−14.9%
NO_3^-	20.8	21.2	0.91	0.36	1.7%
NH_4^+	12.2	9.4	0.89	−2.80	−23.0%
BC	2.3	2.2	0.87	−0.04	−1.9%
OC	21.7	16.7	0.80	−5.06	−23.3%

substances around BC, which can act as a lens to focus more light on the core and enhance absorption of aerosols).[61–63]

Table 3 presents the model performance statistics for AOD and SSA at 550 nm in the four sensitivity cases at the two sites. In general, the model reproduces the day-to-day AOD variation quite well in the four cases, with *R* of around 0.8; however, the predicted AOD is approximately 20% lower than the observation in the EXT case, whereas the NMBs for AOD are less than 2% in the other cases, with the least bias in the M-G case. It is noteworthy that SSA is overpredicted (1.7%) and underpredicted (−2.3%) in the EXT and HOM cases, respectively, which means that the absorption ability of aerosols is underestimated and overestimated, respectively, whereas the biases in the M-G and C–S cases are very close (0.5%) and smaller than that in the other cases. *R* for SSA in the HOM case is apparently lower than those in the other cases. The larger biases in AOD and SSA in the EXT and HOM cases suggest that these two mixing states could not represent the actual mixing state of aerosols in the atmosphere during the study period. In all, the assumption of core–shell-type internal mixing (including M-G mixing, which is also a core–shell type with the position of the core unfixed) leads to better agreement between the model simulations and observations, and the simulated SSA in the M-G case agrees better with observations than that in the C–S case, especially during the haze episode, with respect to the comparison on 9–12 at Beijing-RADI (Fig. 3c).

3.2 Aerosol direct radiative effects under various aerosol mixing states

Because the cloud amount and precipitation were relatively low during the study period (as well as during the haze episode), only the aerosol direct radiative effect and feedback are discussed in this study. Fig. 4 shows the period-mean DRE at the top of the atmosphere (TOA), at the surface (SUF), and in the atmosphere (ATM, TOA minus SUF) over NCP during the haze episode of 8–13 February 2020, in the four sensitivity cases. It clearly shows that anthropogenic aerosols induced a negative DRE at TOA and at the surface, and a positive DRE in the atmosphere with stronger magnitudes over the areas from Beijing and Tianjin to the southern parts of the domain in all cases. It is found that the DREs in these cases are consistent with each other in distribution pattern, but differ largely in magnitude. The HOM case exhibits the maximum DRE at the

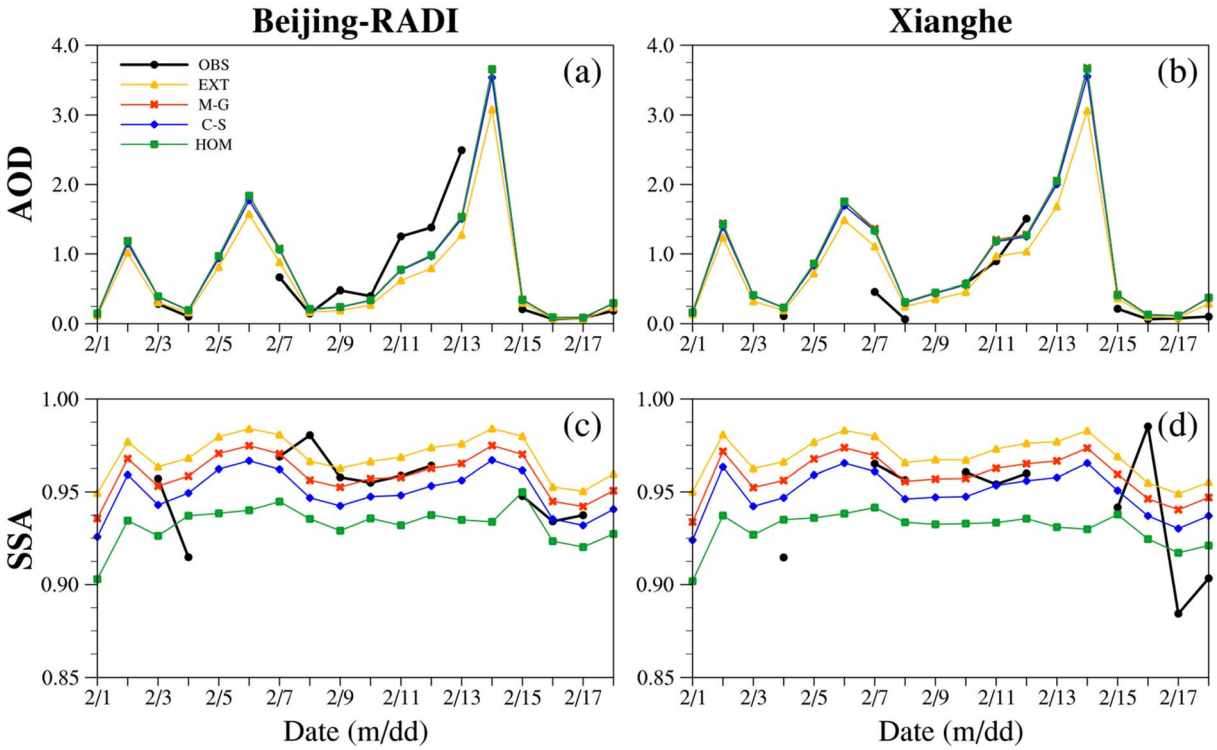

Fig. 3 Model-simulated (with the four mixing states) and observed daily mean AOD (a and b) and SSA (c and d) at 550 nm at Beijing-RADI (a and c) and Xianghe (b and d) from 1 to 18 February, 2020.

surface and in the atmosphere, followed by the C–S and M-G cases, whereas the EXT case exhibits the minimum DRE.

DRE at TOA in the HOM case is the weakest among the cases due to the maximum positive DRE in the atmosphere, which means more solar radiation is absorbed in the atmosphere, and less radiation is reflected back to space. In terms of domain average, the DREs at TOA vary from -8.2 W m^{-2} (EXT) to -6.6 W m^{-2} (HOM), which means that the DRE-induced cooling of the surface-atmosphere can differ by 24% across the four mixing states over the NCP region. At the surface, the DRE (-15.5 W m^{-2}) in the HOM case is the maximum among the cases, followed by that in the M-G and C–S cases, and the minimum is in the EXT case. The percentage difference in DRE at the surface among these cases is 40%, which is larger than that at TOA. The largest difference in DRE among the cases occurs in the atmosphere, varying from 2.9 W m^{-2} (EXT) to 8.9 W m^{-2} (HOM), and demonstrating that the radiative heating in the atmosphere in the HOM case is approximately three-times that in the EXT case. The above-mentioned model results demonstrate that the mixing states of aerosols can result in large differences in the magnitude of DRE, with the maximum DRE difference in the atmosphere, and this could result in large differences in the aerosol radiative feedback on the meteorology and particulate matter levels, which will be discussed in the next section.

3.3 The effect of size distribution, coating fraction and hygroscopic growth on AOD, SSA and DRE

Aerosol optical properties can be affected by a series of physical and environmental factors. Based on the M-G experiment (showing the best agreement with observations), three additional sensitivity tests were conducted to explore the effect of BC size, coating fraction and hygroscopic growth on aerosol optical properties and DRE. In the M-G case, the typical BC size is set to

Table 3 Model performance statistics for daily mean AOD and SSA in the four cases at the Beijing-RADI and Xianghe sites during the study period from 1 to 18 February 2020

	AOD					SSA (%)				
Mixing states	Obs	Sim	*R*	MB	NMB	Obs	Sim	*R*	MB	NMB
EXT	0.49	0.39	0.81	−0.10	−19.5%	94.6	96.2	0.40	1.57	1.7%
M-G	0.49	0.49	0.81	0.00	0.0%	94.6	95.1	0.36	0.52	0.6%
C–S	0.49	0.48	0.81	−0.01	−1.7%	94.6	94.2	0.36	−0.43	−0.5%
HOM	0.49	0.49	0.82	0.00	−0.3%	94.6	92.4	0.28	−2.19	−2.3%

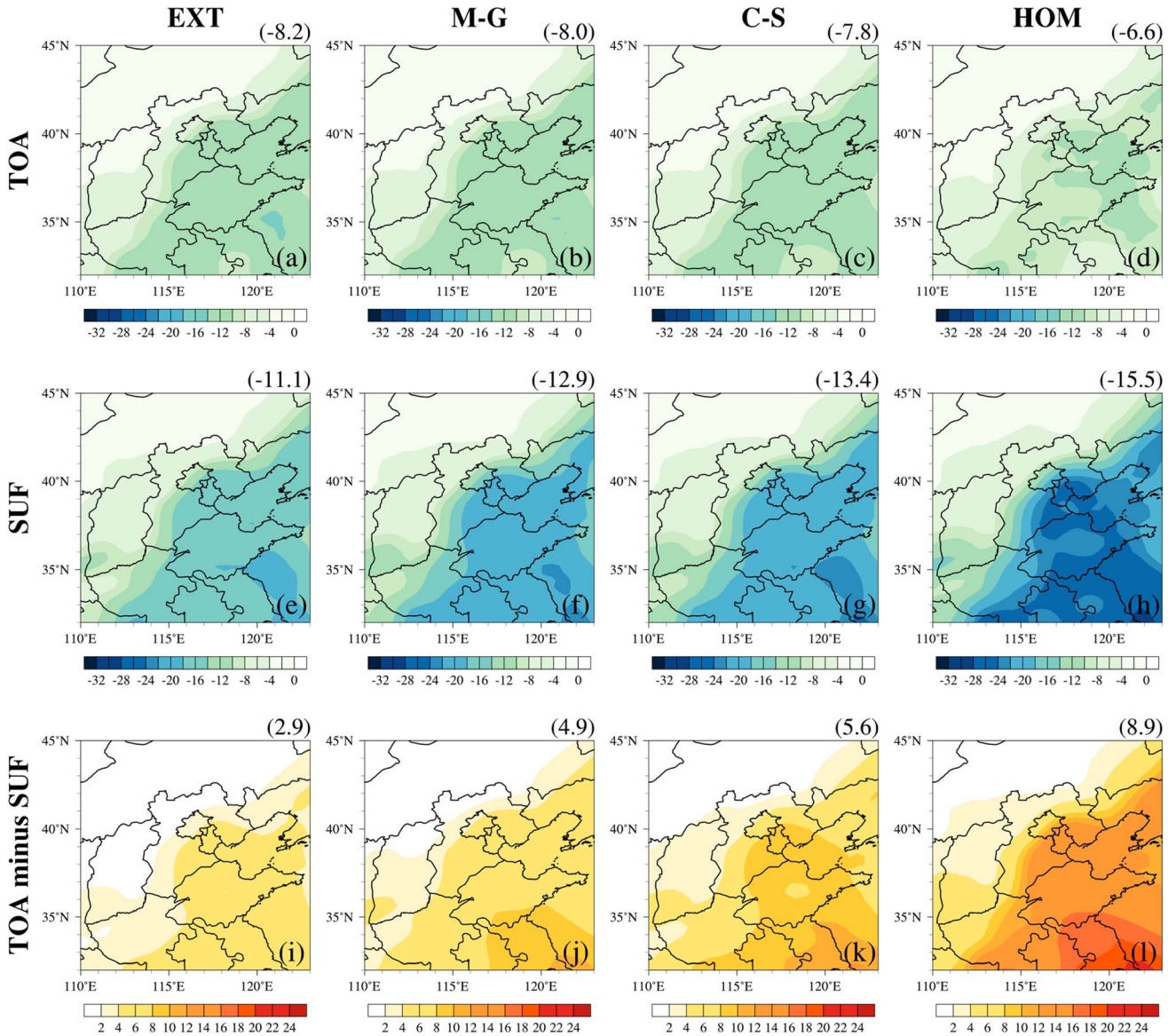

Fig. 4 Model-simulated period-mean DREs at TOA (a–d), at the surface (e–h), and in the atmosphere (i–l) during the haze episode on 8–13 February 2020, in the four sensitivity cases regarding various mixing states. The numbers in the upper-right corner of each panel represent the domain average values (unit: W m^{-2}).

0.2 μm according to observational analysis in winter in Beijing.[26] Wu *et al.*[64] analyzed the variation in BC size distribution during 2013–2019 in Beijing, and revealed a decreasing trend in BC size under emission control, and thus in TEST1, a typical BC size of 0.16 μm is assumed. In the M-G case, it assumes that all the scattering aerosols (sulfate, nitrate, and SOA) coat BC; however, Wu *et al.*[25] indicated that approximately 70% of aerosols are core–shell mixing on BC during haze episodes, and thus in TEST2, we assume 70% scattering aerosols coated on BC, with the remaining mixing externally. In TEST3, it is assumed that hygroscopic growth is not considered. Fig. S3 shows the simulated AOD (including total AOD, scattering and absorbing AOD) and SSA during the study period in Beijing-RADI (corresponding to Fig. 3a and c, respectively) in the M-G and the three test cases. Compared with M-G, the scattering and absorption coefficients both decrease in TEST1, leading to a decrease in total AOD; however, the decrease in scattering is larger than that in absorption, resulting in a decrease in SSA. In TEST2, while 30% of scattering aerosols do not coat BC, retaining their own properties as external mixing, the absorption decreases due to the thinner shell and weaker lensing effect, and the scattering coefficient also decreases due to the smaller sizes of both the core–shell and external mixed aerosols, with their combined effect leading to a decrease in AOD. Meanwhile, the decrease in absorption is larger than that in scattering, leading to an increase in SSA. In TEST3 ignoring hygroscopic growth, scattering decreases largely due to the decrease in size, while absorption also decreases due to the thinner shell and weaker lensing effect, which cause an apparent decrease in AOD; because the decrease in scattering is much larger than that in

absorption, SSA decreases considerably compared to the M-G case. It is noted that the changes in AOD and SSA in TEST3 are larger than that in TEST1 and TEST2, indicating the significance of hygroscopic growth in determining aerosol optical properties.

Correspondingly, Fig. S4 shows the simulated DRE in the M-G and the three test cases. In general, the DREs in the three test cases are all weaker than that in the M-G case. Compared with M-G, TEST3 shows an evident decrease in DRE by approximately 39%, 31% and 18% at TOA, at the surface and in the atmosphere, respectively, which is larger than the DRE decrease in the other two cases.

3.4 Aerosol radiative feedback on meteorology and $PM_{2.5}$ levels under various mixing states

Fig. 5 presents the model-simulated period-mean radiative feedback-induced changes in T2, RH2, WS10, planetary boundary layer height (PBLH), and near-surface $PM_{2.5}$ concentration in the four sensitivity cases during the haze episode of 8–13 February. It is clearly seen that the spatial distributions of the changes induced by aerosol radiative feedback are alike among these cases and the aerosol DRE induces negative changes in T2, WS10, and PBLH, and positive changes in RH2 and $PM_{2.5}$ concentration.

Generally, it is noted that the stronger DRE, the greater the decrease in T2 due to the larger reduction in shortwave radiation at the surface. The maximum T2 decrease in the domain ranges from 0.66 °C in EXT to 0.86 °C in HOM (numbers in the upper-left corners of each panel), which is about 0.2 °C difference among the cases. The maximum increase and decrease in RH2 and WS10 in the domain range from 5% to 5.6%, and 0.16 to 0.22 m s^{-1}, respectively, in the four cases. In response to the above-mentioned changes, PBLH decreases by 75.8 m and 94.3 m in EXT and HOM, respectively, differing by approximately 19 m among the four cases. The meteorological changes induced by aerosol DRE feedback on $PM_{2.5}$ concentration through both physical and chemical processes.[18] It is noteworthy that the maximum increase in near-surface $PM_{2.5}$ concentration in the domain varies from 21.2 μg m^{-3} in EXT to 29 μg m^{-3} in HOM, indicating that different aerosol mixing states can cause approximately 8 μg m^{-3} difference in near-surface $PM_{2.5}$ concentration on average during the 6-day haze episode. Compared to CASE0 (without considering aerosol radiative feedback), the maximum percentage increase in $PM_{2.5}$ concentration in the domain due to the radiative feedback varies from 13% (EXT) to 18% (HOM) averaged over the 6-day haze episode.

In terms of domain average (numbers in the upper-right corners of each panel in Fig. 5), the difference in the radiative feedback-induced meteorological and $PM_{2.5}$ changes among the cases is smaller compared with the difference in the maximum changes in the domain. It is noteworthy that the magnitude of meteorological changes is not the largest in HOM, *e.g.*, the domain-average decrease in T2 in HOM (−0.25 °C) is slightly lower than that in other cases, which is caused by the slight T2 increase in some parts of the southern domain (northern Anhui Province) (Fig. 5p), partly offsetting the T2 decrease in most areas of the domain. The slight increase in T2 in the above-mentioned areas could be attributed to atmospheric shortwave heating near the surface. Fig. 6 presents the spatial distribution of the atmospheric heating rate (AHR) induced by aerosols (compared with CASE0) in the first model layer in the four cases. It clearly shows a high AHR over the regions of higher $PM_{2.5}$ concentrations (Fig. S5d) due to the aerosol absorption of solar radiation. The strongest AHR appears in HOM (Fig. 6d), with the domain-average value of 1.0 K per day, which is about three-times (two times) the values in the EXT and M-G/C–S cases (0.3 K per day and 0.5 K per day, respectively). Fig. S6 shows the vertical profiles of AHR changes induced by aerosols at the cross section of 40°N in the four cases. It is remarkable that AHR is highest in the areas around Beijing, and generally decreases with altitude because anthropogenic aerosols are mainly concentrated near the surface and confined in the boundary layer. It is noted that AHR is largest in HOM (Fig. S6d), and the height to which AHR affects is also the highest (approximately 1000 m) among the cases. The near-surface air temperature is affected by both the DRE-induced cooling and AHR-induced warming. The strong AHR in HOM dominates over the cooling effect, leading to a slight T2 increase in parts of the southern domain (Fig. 5p), while this is not the case under the other mixing states due to the weaker aerosol absorption and AHR. As a result, PBLH increases in parts of the southern domain of T2 increasing (Fig. 5s). However, despite the fact that an increase in PBLH tends to reduce the $PM_{2.5}$ levels in these areas due to the enhanced vertical diffusivity, the $PM_{2.5}$ concentration still slightly increases by radiative feedback (Fig. 5t), which can be attributed to the transport effect of enhanced inorganic aerosols by thermodynamic and heterogeneous chemical reactions with increasing RH (Fig. 5q) from the surrounding areas.

To further explore the extent to which the aerosol mixing states affect the radiative feedback, Table 4 presents the model-simulated (in the four sensitivity cases) daytime mean radiative feedback-induced changes in $PM_{2.5}$ and meteorological variables in the vicinity of Beijing on 12 February, 2020, when the $PM_{2.5}$ concentration reached the maximum value during the haze episode. It is noteworthy that the changes in T2, RH2, WS10 induced by the radiative feedback vary by −1.2–1.4 °C, 5.5–6.2%, and −0.28–0.37 m s^{-1} in these cases, respectively, which are larger in magnitude than the maximum change in the domain in terms of period-mean. As discussed before, the HOM case does not display a stronger feedback effect on T2 and RH2 than the other cases due to complex interplay between radiative cooling and atmospheric heating. The magnitude of wind speed decrease is consistent with the magnitude of DRE in the four cases. The PBLH decreases in the four cases, with the largest decrease in HOM (181 m), followed by M-G and C–S, and the minimum in EXT (161 m), consistent with the magnitude of DRE in these cases as well. The magnitude of $PM_{2.5}$ increase generally follows that of the PBLH decrease in the four cases. It is impressive that the feedback-induced $PM_{2.5}$ increase varies considerably from the minimum of 40.3 μg m^{-3} to the maximum of 57.6 μg m^{-3}, in EXT and HOM, respectively, with about 17 μg m^{-3} difference among the cases. The M-G and C–S

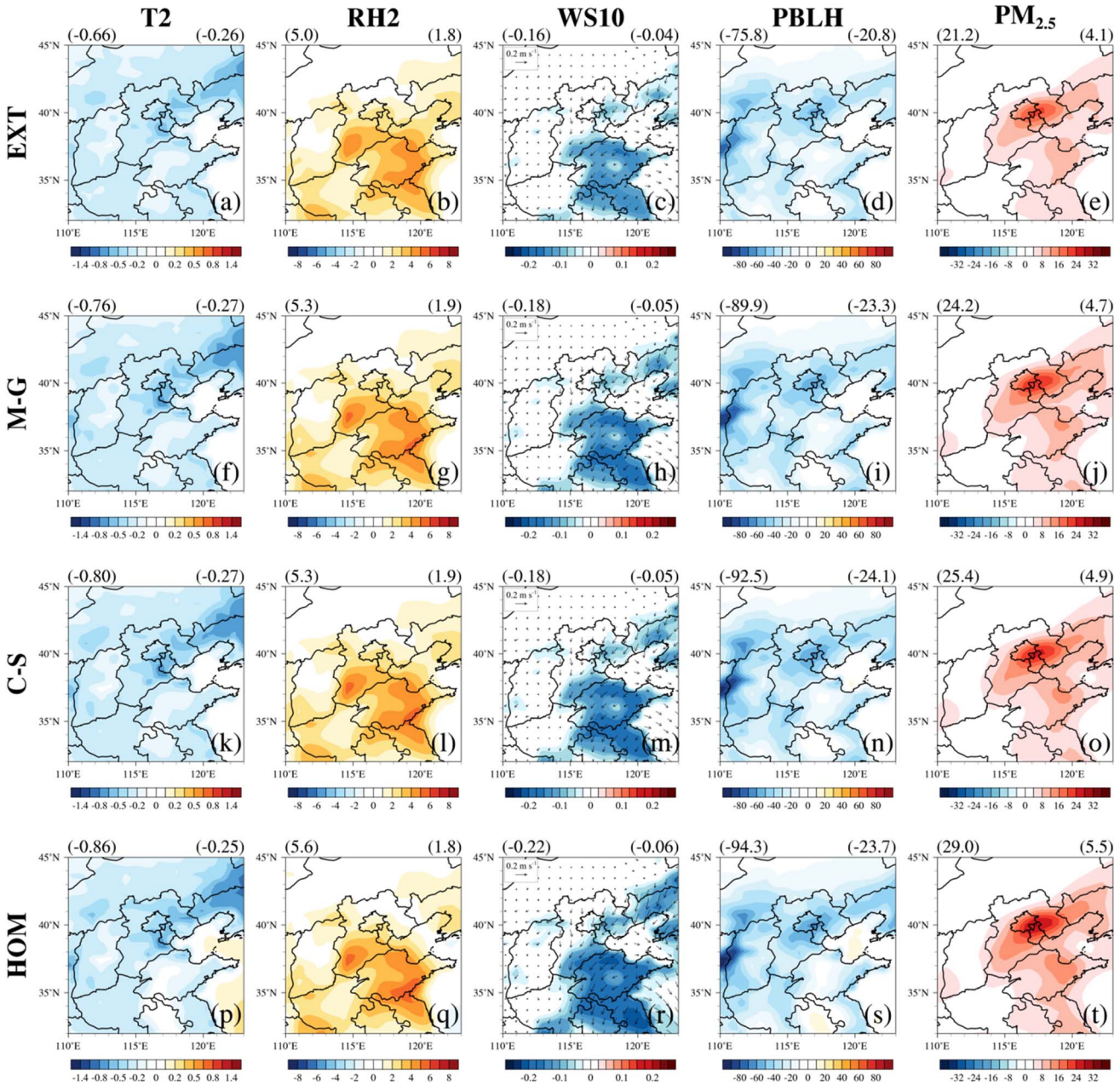

Fig. 5 Model-simulated period-mean radiative feedback-induced changes in T2 (a, f, k, p), RH2 (b, g, l, q), WS10 (c, h, m, r), PBLH (d, i, n, s), and $PM_{2.5}$ concentration (e, j, o, t) during the haze episode on 8–13 February 2020, in the four sensitivity cases. The numbers in the upper-left and upper-right corners of each panel represent the maximum values in the domain and the domain average values, respectively (units, T2: °C, RH2: %, WS10: m s^{-1}, PBLH: m, and $PM_{2.5}$: μg m^{-3}).

cases produce a similar magnitude of $PM_{2.5}$ increase of around 48 μg m^{-3}. With respect to $PM_{2.5}$ concentration in CASE0, the radiative feedback causes a $PM_{2.5}$ increase by 25%, 30%, 30% and 36% in EXT, M-G, C–S and HOM, respectively, which on one hand demonstrates the importance of the radiative feedback in enhancing the $PM_{2.5}$ concentration during the haze episode, and on the other hand indicates the important impact of aerosol mixing states on the feedback effect, which may lead to approximately 11% difference in the feedback-induced $PM_{2.5}$ increase. It is worth emphasizing that the changes in $PM_{2.5}$ concentration are affected by the feedback-induced changes in both meteorological and chemical processes. As mentioned above, RH increased in all cases due to the air temperature decrease or water vapor increase by advection, both of which may enhance the chemical production of inorganic aerosols (through thermodynamic equilibrium and heterogeneous chemical processes), also contributing to the increase in $PM_{2.5}$ concentration besides the effect of PBLH decrease.

The comparison between the 6-day haze episode and the heaviest haze day also exhibits that the difference in the

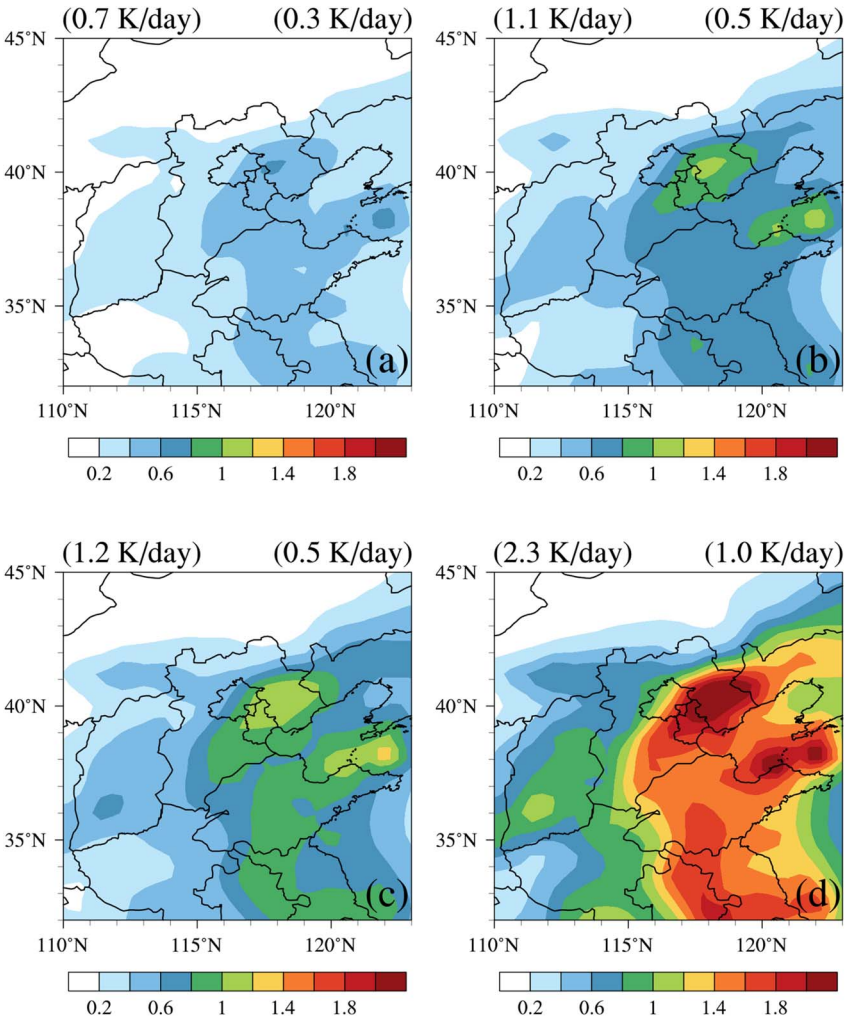

Fig. 6 Model-simulated period-mean aerosol-induced atmospheric hearting rate (AHR, K per day) changes in the first model layer in the four cases (a) EXT, (b) M-G, (c) C–S, and (d) HOM during the haze episode on 8–13 February 2020. The numbers in the upper-left and upper-right corners of each panel represent the maximum and average values in the domain, respectively.

Table 4 Model-simulated T2 (°C), RH2 (%), WS10 (m s^{-1}), PBLH (m), and $PM_{2.5}$ concentration (μg m^{-3}) in CASE0 and the feedback-induced meteorological and $PM_{2.5}$ changes in the four cases in the vicinity of Beijing (39.6°N, 116.6°E), averaged over the daytime period (10:00–17:00) on 12 February 2020

Case	T2	RH2	WS10	PBLH	$PM_{2.5}$
CASE0	10.2	67.9	1.6	678.0	160.9
EXT	−1.3	5.9	−0.28	−160.8	40.3
M-G	−1.4	6.2	−0.31	−176.8	48.1
C–S	−1.3	6.2	−0.32	−178.0	48.4
HOM	−1.2	5.5	−0.37	−181.0	57.6

feedback-induced $PM_{2.5}$ increase among the cases tends to increase with pollution severity (or $PM_{2.5}$ levels), which suggests that the impact of the aerosol mixing state on the radiative feedback effect will be even stronger during more serious air pollution events (including haze events from both anthropogenic origins and natural origins, *e.g.*, wild fire and dust storm).

4. Conclusions

The aerosol direct radiative effects and feedback on meteorology and near-surface $PM_{2.5}$ concentration under various aerosol mixing states during the haze episode of 8–13 February 2020 were investigated by applying an online-coupled regional climate-chemistry-aerosol model (RIEMS-Chem). Four sensitivity cases with different aerosol mixing state assumptions and treatments, namely external mixing, Maxwell-Garnett internal mixing, core–shell internal mixing, and homogeneous internal mixing, are employed to explore the impact of mixing states on aerosol radiative feedback. Model validation against observations demonstrates the overall good ability of the model in simulating the meteorological variables, $PM_{2.5}$ and its components, and optical properties. The simulated AOD with the four mixing states except external mixing is close to each other, while the EXT case underpredicts AOD by about 20%. The simulated SSA differs largely, with the highest SSA in the EXT case, followed by the M-G and C–S cases, and the HOM case yields the

lowest SSA. The simulated SSA with the core–shell-type internal mixing (including M-G and C–S mixing) agrees better with observations than that with the EXT and HOM mixing. The sensitivity of aerosol optical properties and DRE to the black carbon size distribution and coating fraction, and hygroscopic growth under Maxwell-Garnett mixing are also investigated, showing the remarkable effect of hygroscopic growth.

Anthropogenic aerosols induce stronger radiative effects from Beijing and Tianjin to the southern parts of NCP in all cases. The DREs in the four cases are consistent with each other in distribution pattern, but differ largely in magnitude. During the haze episode of 8–13 February, in terms of domain average, the percentage differences in DRE at TOA and at the surface among the cases are 24% and 40%, respectively, while the largest DRE difference occurs in the atmosphere.

Aerosol DRE induces negative changes in T2, WS10, and PBLH, and positive changes in RH2 and $PM_{2.5}$ concentration. Averaged over the 6-day haze episode, the maximum decrease in T2 and WS10, and the maximum increase in RH2 in the domain range from 0.66 °C to 0.86 °C, 0.16 to 0.22 m s^{-1}, and 5% to 5.6% in the four cases, and the PBLH decrease and $PM_{2.5}$ increase differ by approximately 19 m and 8 μg m^{-3} in these cases, respectively. Although surface cooling/warming tends to reduce/increase PBLH and favor/against pollutant accumulation, lower temperature and higher RH enhance the chemical formation of inorganic aerosols, and thus increase the $PM_{2.5}$ concentrations. It is noteworthy that the radiative feedback does not cause consistent surface cooling in the entire domain in all the mixing cases. In the HOM case, T2 and PBLH increase in portions of southern NCP due to the strongest aerosol-induced AHR among the cases, which dominates over the DRE-induced surface cooling, and this tends to reduce the near surface $PM_{2.5}$ concentrations.

During the severest haze day, the changes in T2, RH2, and WS10 induced by the feedback vary by −1.2–1.4 °C, 5.5–6.2%, and −0.28–0.37 m s^{-1} in these cases, respectively, in the vicinity of Beijing. It is noteworthy that the feedback-induced $PM_{2.5}$ increase differs by approximately 17 μg m^{-3} among the four mixing states. The radiative feedback results in an increase in $PM_{2.5}$ concentration by 25%, 30%, 30% and 36% in EXT, M-G, C–S and HOM relative to CASE0, respectively, demonstrating the importance of radiative feedback in enhancing the $PM_{2.5}$ level and the large difference in the feedback-induced $PM_{2.5}$ increase across the mixing states during the haze episode.

Although this study demonstrates the significant impact of aerosol mixing states on aerosol optical and radiative properties, and thus on the radiative feedback on meteorology and $PM_{2.5}$ concentrations, it is still subject to some limitations. (1) The model underpredicts the organic aerosol concentration by approximately 20%, which could somewhat underestimate the magnitude of aerosol radiative feedback and mixing state impact. (2) The assumption for each mixing state is applied for the entire study period, but in reality, the mixing state varies during aging processes from clean to polluted conditions. (3) This study focuses on a haze episode in winter when cloud and precipitation are limited, and thus the aerosol indirect effect and its relation with the mixing states were not investigated. It is expected that the aerosol mixing state evolution along with air quality processing, the potential impacts of aerosol mixing states on CCN, cloud droplet activation, and aerosol indirect radiative effects will continue to be explored together with more laboratory and field observations, and model development in the future.

Conflicts of interest

The corresponding author has declared that the authors have no competing interests.

Data availability

The observational and modeling data will be available from the corresponding author upon request.

Supplementary information (SI): Table S1 and Fig. S1–S6. See DOI: https://doi.org/10.1039/d5ea00126a.

Acknowledgements

This study was supported by the National Natural Science Foundation of China (no. 42375107 and 42275118).

References

1 S. Twomey, Pollution and the planetary albedo, *Atmos. Environ.*, 1974, **8**, 1251–1256.
2 B. A. Albrecht, Aerosols, Cloud Microphysics, and Fractional Cloudiness, *Science*, 1989, **245**, 1227–1230.
3 V. Ramanathan, P. J. Crutzen, J. T. Kiehl and D. Rosenfeld, Aerosols, Climate, and the Hydrological Cycle, *Science*, 2001, **294**, 2119–2124.
4 A. Baklanov, K. Schluenzen, P. Suppan, J. Baldasano, D. Brunner, S. Aksoyoglu, G. Carmichael, J. Douros, J. Flemming, R. Forkel, S. Galmarini, M. Gauss, G. Grell, M. Hirtl, S. Joffre, O. Jorba, E. Kaas, M. Kaasik, G. Kallos, X. Kong, U. Korsholm, A. Kurganskiy, J. Kushta, U. Lohmann, A. Mahura, A. Manders-Groot, A. Maurizi, N. Moussiopoulos, S. T. Rao, N. Savage, C. Seigneur, R. S. Sokhi, E. Solazzo, S. Solomos, B. Sorensen, G. Tsegas, E. Vignati, B. Vogel and Y. Zhang, Online coupled regional meteorology chemistry models in Europe: current status and prospects, *Atmos. Chem. Phys.*, 2014, **14**, 317–398.
5 U. Im, R. Bianconi, E. Solazzo, I. Kioutsioukis, A. Badia, A. Balzarini, R. Baró, R. Bellasio, D. Brunner, C. Chemel, G. Curci, H. D. van der Gon, J. Flemming, R. Forkel, L. Giordano, P. Jiménez-Guerrero, M. Hirtl, A. Hodzic, L. Honzak, O. Jorba, C. Knote, P. A. Makar, A. Manders-Groot, L. Neal, J. L. Pérez, G. Pirovano, G. Pouliot, R. San Jose, N. Savage, W. Schroder, R. S. Sokhi, D. Syrakov, A. Torian, P. Tuccella, K. Wang, J. Werhahn, R. Wolke, R. Zabkar, Y. Zhang, J. H. Zhang, C. Hogrefe and S. Galmarini, Evaluation of operational online-coupled regional air quality models over Europe and North America in the context of AQMEII phase 2. Part II: particulate matter, *Atmos. Environ.*, 2015, **115**, 421–441.

6 R. S. Sokhi, N. Moussiopoulos, A. Baklanov, J. Bartzis, I. Coll, S. Finardi, R. Friedrich, C. Geels, T. Grönholm, T. Halenka, M. Ketzel, A. Maragkidou, V. Matthias, J. Moldanova, L. Ntziachristos, K. Schäfer, P. Suppan, G. Tsegas, G. Carmichael, V. Franco, S. Hanna, J. P. Jalkanen, G. J. M. Velders and J. Kukkonen, Advances in air quality research - current and emerging challenges, *Atmos. Chem. Phys.*, 2022, **22**, 4615–4703.

7 J. D. Wang, S. X. Wang, J. K. Jiang, A. J. Ding, M. Zheng, B. Zhao, D. C. Wong, W. Zhou, G. J. Zheng, L. Wang, J. E. Pleim and J. M. Hao, Impact of aerosol-meteorology interactions on fine particle pollution during China's severe haze episode in January 2013, *Environ. Res. Lett.*, 2014, **9**, 094002.

8 Z. Wang, J. Li, Z. Wang, W. Yang, X. Tang, B. Ge, P. Yan, L. Zhu, X. Chen, H. Chen, W. Wand, J. Li, B. Liu, X. Wang, W. Wand, Y. Zhao, N. Lu and D. Su, Modeling study of regional severe hazes over mid-eastern China in January 2013 and its implications on pollution prevention and control, *Sci. China Earth Sci.*, 2014, **57**, 3–13.

9 B. Zhang, Y. Wang and J. Hao, Simulating aerosol-radiation-cloud feedbacks on meteorology and air quality over eastern China under severe haze conditions in winter, *Atmos. Chem. Phys.*, 2015, **15**, 2387–2404.

10 Y. Gao, M. Zhang, Z. Liu, L. Wang, P. Wang, X. Xia, M. Tao and L. Zhu, Modeling the feedback between aerosol and meteorological variables in the atmospheric boundary layer during a severe fog–haze event over the North China Plain, *Atmos. Chem. Phys.*, 2015, **15**, 4279–4295.

11 M. Gao, G. R. Carmichael, Y. Wang, P. E. Saide, M. Yu, J. Xin, Z. Liu and Z. Wang, Modeling study of the 2010 regional haze event in the North China Plain, *Atmos. Chem. Phys.*, 2016, **16**, 1673–1691.

12 Y. L. Qiu, H. Liao, R. J. Zhang and J. L. Hu, Simulated impacts of direct radiative effects of scattering and absorbing aerosols on surface layer aerosol concentrations in China during a heavily polluted event in February 2014, *J. Geophys. Res. Atmos.*, 2017, **122**, 5955–5975.

13 B. Zhao, K. N. Liou, Y. Gu, Q. B. Li, J. H. Jiang, H. Su, C. L. He, H. L. R. Tseng, S. X. Wang, R. Liu, L. Qi, W. L. Lee and J. M. Hao, Enhanced $PM_{2.5}$ pollution in China due to aerosol-cloud interactions, *Sci. Rep.*, 2017, **7**, 4453.

14 X. Huang, Z. Wang and A. Ding, Impact of Aerosol-PBL Interaction on Haze Pollution: Multi-Year Observational Evidences in North China, *Geophys. Res. Lett.*, 2018, **45**, 8596–8603.

15 X. Zhang, Q. Zhang, C. P. Hong, Y. X. Zheng, G. N. Geng, D. Tong, Y. X. Zhang and X. Y. Zhang, Enhancement of $PM_{2.5}$ Concentrations by Aerosol-Meteorology Interactions Over China, *J. Geophys. Res. Atmos.*, 2018, **123**, 1179–1194.

16 J. T. Zhong, X. Y. Zhang, Y. S. Dong, Y. Q. Wang, C. Liu, J. Z. Wang, Y. M. Zhang and H. C. Che, Feedback effects of boundary-layer meteorological factors on cumulative explosive growth of $PM_{2.5}$ during winter heavy pollution episodes in Beijing from 2013 to 2016, *Atmos. Chem. Phys.*, 2018, **18**, 247–258.

17 J. R. Wu, N. F. Bei, B. Hu, S. X. Liu, M. Zhou, Q. Y. Wang, X. Li, L. Liu, T. Feng, Z. R. Liu, Y. C. Wang, J. J. Cao, X. X. Tie, J. Wang, L. T. Molina and G. H. Li, Aerosol-radiation feedback deteriorates the wintertime haze in the North China Plain, *Atmos. Chem. Phys.*, 2019, **19**, 8703–8719.

18 J. W. Li, Z. W. Han, Y. F. Wu, Z. Xiong, X. G. Xia, J. Li, L. Liang and R. J. Zhang, Aerosol radiative effects and feedbacks on boundary layer meteorology and $PM_{2.5}$ chemical components during winter haze events over the Beijing-Tianjin-Hebei region, *Atmos. Chem. Phys.*, 2020, **20**, 8659–8690.

19 M. Gao, Z. Han, Z. Tao, J. Li, J. E. Kang, K. Huang, X. Dong, B. Zhuang, S. Li, B. Ge, Q. Wu, H. J. Lee, C. H. Kim, J. S. Fu, T. Wang, M. Chin, M. Li, J. H. Woo, Q. Zhang, Y. Cheng, Z. Wang and G. R. Carmichael, Air quality and climate change, Topic 3 of the Model Inter-Comparison Study for Asia Phase III (MICS-Asia III) – Part 2: aerosol radiative effects and aerosol feedbacks, *Atmos. Chem. Phys.*, 2020, **20**, 1147–1161.

20 Y. Gao, B. Zhuang, T. Wang, H. Chen, S. Li, W. Wei, H. Lin and M. Li, Climatic–Environmental Effects of Aerosols and Their Sensitivity to Aerosol Mixing States in East Asia in Winter, *Remote Sens.*, 2022, **14**, 3539.

21 M. Jacobson, A physically-based treatment of elemental carbon optics: Implications for global direct forcing of aerosols, *Geophys. Res. Lett.*, 2000, **27**, 217–220.

22 N. Riemer, A. P. Ault, M. West, R. L. Craig and J. H. Curtis, Aerosol Mixing State: Measurements, Modeling, and Impacts, *Rev. Geophys.*, 2019, **57**, 187–249.

23 Y. Y. Wang, Z. H. Zheng, Y. Sun, Y. Yao, P. L. Ma, A. X. Zhang, S. P. Zhu, Z. X. Zhang, X. Y. Chen, Y. E. Pang, Q. Y. Wang, H. Z. Che, J. S. Ching and W. J. Li, Improved representation of black carbon mixing structures suggests stronger direct radiative heating, *One Earth*, 2025, **8**, 101311.

24 N. Ma, C. S. Zhao, T. Müller, Y. F. Cheng, P. F. Liu, Z. Z. Deng, W. Y. Xu, L. Ran, B. Nekat, D. van Pinxteren, T. Gnauk, K. Müeller, H. Herrmann, P. Yan, X. J. Zhou and A. Wiedensohler, A new method to determine the mixing state of light absorbing carbonaceous using the measured aerosol optical properties and number size distributions, *Atmos. Chem. Phys.*, 2012, **12**, 2381–2397.

25 Y. F. Wu, R. J. Zhang, P. Tian, J. Tao, S. C. Hsu, P. Yan, Q. Y. Wang, J. J. Cao, X. L. Zhang and X. G. Xia, Effect of ambient humidity on the light absorption amplification of black carbon in Beijing during January 2013, *Atmos. Environ.*, 2016, **124**, 217–223.

26 Y. F. Wu, X. J. Wang, J. Tao, R. J. Huang, P. Tian, J. J. Cao, L. M. Zhang, K. F. Ho, Z. W. Han and R. J. Zhang, Size distribution and source of black carbon aerosol in urban Beijing during winter haze episodes, *Atmos. Chem. Phys.*, 2017, **17**, 7965–7975.

27 Q. Y. Wang, L. Li, J. M. Zhou, J. H. Ye, W. T. Dai, H. K. Liu, Y. Zhang, R. J. Zhang, J. Tian, Y. Chen, Y. F. Wu, W. K. Ran and J. J. Cao, Measurement report: Source and mixing state of black carbon aerosol in the North China Plain: implications for radiative effect, *Atmos. Chem. Phys.*, 2020, **20**, 15427–15442.

28 J. Y. Liu, F. Zhang, J. Y. Ren, L. Chen, A. R. Zhang, Z. Wang, S. J. Zou, H. H. Xu and X. Y. Yue, The evolution of aerosol mixing state derived from a field campaign in Beijing: implications for particle aging timescales in urban atmospheres, *Atmos. Chem. Phys.*, 2025, **25**, 5075–5086.

29 Q. Zhang, Y. X. Zheng, D. Tong, M. Shao, S. X. Wang, Y. H. Zhang, X. D. Xu, J. N. Wang, H. He, W. Q. Liu, Y. H. Ding, Y. Lei, J. H. Li, Z. F. Wang, X. Y. Zhang, Y. S. Wang, J. Cheng, Y. Liu, Q. R. Shi, L. Yan, G. N. Geng, C. P. Hong, M. Li, F. Liu, B. Zheng, J. J. Cao, A. J. Ding, J. Gao, Q. Y. Fu, J. T. Huo, B. X. Liu, Z. R. Liu, F. M. Yang, K. B. He and J. M. Hao, Drivers of improved $PM_{2.5}$ air quality in China from 2013 to 2017, *Proc. Natl. Acad. Sci. U. S. A.*, 2019, **116**, 24463–24469.

30 Y. Li, Z. W. Han, Y. Song, J. W. Li, Y. L. Sun and T. T. Wang, Impacts of the COVID-19 lockdown on atmospheric oxidizing capacity and secondary aerosol formation over the Beijing-Tianjin-Hebei region in Winter-Spring 2020, *Atmos. Environ.*, 2023, **295**, 119540.

31 C. Fu, S. Wang, Z. Xiong, W. J. Gutowski, D. K. Lee, J. L. McGregor, Y. Sato, H. Kato, J. W. Kim and M. S. Suh, Regional climate model intercomparison project for Asia, *Bull. Am. Meteorol. Soc.*, 2005, **86**, 257–266.

32 S. Y. Wang, C. B. Fu, H. L. Wei, Y. Qian, Z. Xiong, J. M. Feng, D. M. Zhao, L. Dan, Z. W. Han, B. K. Su, M. Zhao, Y. C. Zhang, J. P. Tang, H. N. Liu, J. Wu, X. M. Zeng, M. Chen and L. Z. Wang, Regional integrated environmental modeling system: development and application, *Clim. Change*, 2015, **129**, 499–510.

33 Z. Han, Direct radiative effect of aerosols over East Asia with a Regional coupled Climate/Chemistry model, *Meteorol. Z.*, 2010, **19**, 287–298.

34 Z. Han, J. Li, X. Xia and R. Zhang, Investigation of direct radiative effects of aerosols in dust storm season over East Asia with an online coupled regional climate-chemistry-aerosol model, *Atmos. Environ.*, 2012, **54**, 688–699.

35 J. W. Li and Z. W. Han, Aerosol vertical distribution over east China from RIEMS-Chem simulation in comparison with CALIPSO measurements, *Atmos. Environ.*, 2016, **143**, 177–189.

36 M. W. Gery, G. Z. Whitten, J. P. Killus and M. C. Dodge, A photochemical kinetics mechanism for urban and regional scale computer modeling, *J. Geophys. Res.*, 1989, **94**, 12925–12956.

37 J. Lee-Taylor and S. Madronich, Climatology of UV-A, UV-B, and erythemal radiation at the earth's surface, 1979–2000, *NCAR Technical Note*, NCAR/TN-474+STR, 2007, pp. 1–52.

38 C. Fountoukis and A. Nenes, ISORROPIA II: a computationally efficient thermodynamic equilibrium model for K^+–Ca^{2+}–Mg^{2+}–NH_4^+–Na^+–SO_4^{2-}–NO_3^-–Cl^-–H_2O aerosols, *Atmos. Chem. Phys.*, 2007, **7**, 4639–4659.

39 J. R. Odum, T. P. W. Jungkamp, R. J. Griffin, R. C. Flagan and J. H. Seinfeld, The atmospheric aerosol-forming potential of whole gasoline vapor, *Science*, 1997, **276**, 96–99.

40 J. W. Li and Z. W. Han, A modeling study of the impact of heterogeneous reactions on mineral aerosol surfaces on tropospheric chemistry over East Asia, *Particuology*, 2010, **8**, 433–441.

41 J. Li, X. S. Chen, Z. F. Wang, H. Y. Du, W. Y. Yang, Y. L. Sun, B. Hu, J. J. Li, W. Wang, T. Wang, P. Q. Fu and H. L. Huang, Radiative and heterogeneous chemical effects of aerosols on ozone and inorganic aerosols over East Asia, *Sci. Total Environ.*, 2018, **622**, 1327–1342.

42 J. W. Li, Z. W. Han and X. H. Yao, A modeling study of the influence of sea salt on inorganic aerosol concentration, size distribution, and deposition in the western Pacific Ocean, *Atmos. Environ.*, 2018, **188**, 157–173.

43 Z. Han, H. Ueda, K. Matsuda, R. Zhang, K. Arao, Y. Kanai and H. Hasome, Model study on particle size segregation and deposition during Asian dust events in March 2002, *J. Geophys. Res.*, 2004, **109**, D19205.

44 M. Hess, P. Koepke and I. Schult, Optical properties of aerosols and clouds: The software package OPAC, *Bull. Am. Meteorol. Soc.*, 1998, **79**, 831–844.

45 S. Gong, L. Barrie and J. P. Blanchet, Modeling sea-salt aerosols in the atmosphere .1. Model development, *J. Geophys. Res.*, 1997, **102**, 3805–3818.

46 M. D. Petters and S. M. Kreidenweis, A single parameter representation of hygroscopic growth and cloud condensation nucleus activity, *Atmos. Chem. Phys.*, 2007, **7**, 1961–1971.

47 J. C. M. Garnett, Colours in Metal Glasses and in Metallic Films, *Philos. Trans. R. Soc., A*, 1904, **203**, 385–420.

48 G. A. Niklasson, C. G. Granqvist and O. Hunderi, Effective medium models for the optical properties of inhomogeneous materials, *Appl. Opt.*, 1981, **20**, 26–30.

49 C. F. Bohren and D. R. Huffman, Appendix B: Coated Sphere, in *Absorption and Scattering of Light by Small Particles*, Wiley-VCH Verlag GmbH, Weinheim, Germany, 1998.

50 Z. Han, J. Li, W. Guo, Z. Xiong and W. Zhang, A study of dust radiative feedback on dust cycle and meteorology over East Asia by a coupled regional climate-chemistry-aerosol model, *Atmos. Environ.*, 2013, **68**, 54–63.

51 Z. Han, J. Li, X. Yao and S. Tan, A regional model study of the characteristics and indirect effects of marine primary organic aerosol in springtime over East Asia, *Atmos. Environ.*, 2019, **197**, 22–35.

52 J. W. Li, Z. W. Han and R. J. Zhang, Influence of aerosol hygroscopic growth parameterization on aerosol optical depth and direct radiative forcing over East Asia, *Atmos. Res.*, 2014, **140**, 14–27.

53 J. W. Li, Z. W. Han, X. H. Yao, Z. X. Xie and S. C. Tan, The distributions and direct radiative effects of marine aerosols over East Asia in springtime, *Sci. Total Environ.*, 2019, **651**, 1913–1925.

54 J. W. Li, Z. W. Han, V. Surapipith, W. X. Fan, N. Thingboonchoo, J. Wu, J. Li, J. Tao, Y. F. Wu, R. Macatangay, S. H. Bran, E. T. Yu, A. Z. Zhang, L. Liang and R. J. Zhang, Direct and indirect effects and feedbacks of biomass burning aerosols over Mainland Southeast Asia and South China in springtime, *Sci. Total Environ.*, 2022, **842**, 156949.

55 J. W. Li, Z. W. Han, P. Q. Fu, X. H. Yao and M. J. Liang, Seasonal characteristics of emission, distribution, and radiative effect of marine organic aerosols over the western Pacific Ocean: an investigation with a coupled regional climate aerosol model, *Atmos. Chem. Phys.*, 2024, **24**, 3129–3161.

56 J. W. Li, Z. W. Han, A. Z. Zhang and Z. Y. Meng, The direct and indirect radiative effects of sea salt aerosols over the western Pacific using an online-coupled regional chemistry-climate model with a developed sea salt emission scheme, *Atmos. Res.*, 2024, **303**, 107325.

57 J. W. Li, Z. W. Han, J. Li and L. Luo, Impacts of vertical distribution of Southeast Asian biomass burning emissions on aerosol distributions and direct radiative effects over East Asia, *Atmos. Environ.*, 2024, **318**, 120211.

58 M. J. Liang, Z. W. Han, J. W. Li, Y. L. Sun, L. Liang and Y. Li, Radiative effects and feedbacks of anthropogenic aerosols on boundary layer meteorology and fine particulate matter during the COVID-19 lockdown over China, *Sci. Total Environ.*, 2023, **862**, 160767.

59 M. Liang, Z. Han, J. Li, Y. Li and L. Liang, Aerosol effects during heat waves in summer 2022 and responses to emission change over China, *npj Clim. Atmos. Sci.*, 2024, **7**, 190.

60 L. Fierce, T. B. Onasch, C. D. Cappa, C. Mazzoleni, S. China, J. Bhandari, P. Davidovits, D. A. Fischer, T. Helgestad, A. T. Lambe, A. J. Sedlacek III, G. D. Smith and L. Wolff, Radiative absorption enhancements by black carbon controlled by particle-to-particle heterogeneity in composition, *Proc. Natl. Acad. Sci. U. S. A.*, 2020, **117**, 5196–5203.

61 J. P. Schwarz, J. R. Spackman, D. W. Fahey, R. S. Gao, U. Lohmann, P. Stier, L. A. Watts, D. S. Thomson, D. A. Lack, L. Pfister, M. J. Mahoney, D. Baumgardner, J. C. Wilson and J. M. Reeves, Coatings and their enhancement of black carbon light absorption in the tropical atmosphere, *J. Geophys. Res.*, 2008, **113**, D03203.

62 H. Zhang, C. Zhou, Z. L. Wang, S. Y. Zhao and J. N. Li, The influence of different black carbon and sulfate mixing methods on their optical and radiative properties, *J. Quant. Spectrosc. Radiat. Transfer*, 2015, **161**, 105–116.

63 M. Zanatta, P. Laj, M. Gysel, U. Baltensperger, S. Vratolis, K. Eleftheriadis, Y. Kondo, P. Dubuisson, V. Winiarek, S. Kazadzis, P. Tunved and H. W. Jacobi, Effects of mixing state on optical and radiative properties of black carbon in the European Arctic, *Atmos. Chem. Phys.*, 2018, **18**, 14037–14057.

64 Y. F. Wu, Y. J. Xia, C. Zhou, P. Tian, J. Tao, R. J. Huang, D. T. Liu, X. Wang, X. G. Xia, Z. W. Han and R. J. Zhang, Effect of source variation on the size and mixing state of black carbon aerosol in urban Beijing from 2013 to 2019: Implication on light absorption, *Environ. Pollut.*, 2021, **270**, 116089.

